

Systematic Investigation of the Residence Time Distribution in a Twin-Screw Extruder for the Continuous Mixing Process of Electrode Slurry in the Battery Cell Production

Simon Otte,* Julia Maelger, Sebastian Schabel, Hermann Nirschl, and Jürgen Fleischer

Due to high scrap rates and manufacturing costs, battery cell production requires continuous process optimization. The potential for material efficiency is particularly high in electrode production, specifically in the mixing process. Challenges in the continuous mixing process are related to automation and traceability of material. As one of the most relevant parameters, the residence time of particles must be known, otherwise it is not possible to make a statement about the traceability of the slurry ingredients. Without knowledge of the residence time distribution (RTD), autonomous process control or traceability of battery cells and their components is not possible. The influence of process and material parameters on the RTD of the continuous mixing process in battery cell production is being systematically investigated. Based on a design of experiment, the mean residence time and the RTD are determined for a graphite-based anode slurry by manipulating the conductivity by adding a tracer. Special attention is given to the properties of the tracer as well as the tracer behavior within the mixing process. The influence of different parameters is analyzed based on the conductivity changes. It is shown that the parameters mass flow and solid content have the greatest influence on the RTD.

as continuous process optimization to reduce the high scrap rates and increase resource efficiency.^[1]

In the mixing process, the first step in electrode production, the electrochemical bases for the cell performance are defined. In this process, active materials (AMs), binder, and conductive agent, e.g., carbon black (CB), are diluted in a solvent.^[2] The purpose of mixing is to break up agglomerates and produce a homogeneous slurry with a specific viscosity.^[1,3] Mixing techniques, intensity, duration, and sequencing are key factors in defining the quality of the slurry influences quality of subsequent production steps.^[3,4] The demands placed on companies by the market and customers require continuous optimization, which is why there is a clear shift from batch to continuous processing in modern plant and process engineering. A continuous process continuously feeds input materials into the system, undergoes constant chemical or physical transformations, and continuously releases output materials.^[5]

1. Introduction


The demand for energy storage solutions and lithium-ion battery cells has grown in recent years. Battery cell manufacturers face increased demand and high price pressure as well

Twin-screw extruders (TSE) are well suited for continuous mixing processes, offering advantages over batch processes, like reduced processing time from hours to minutes, optimized shear rates, greater product consistency, and reduced material waste as well as higher output with lower space requirements.^[3,6–8] A TSE consists of two rotating screws within a cylindrical barrel. Raw material is fed into the screws via a hopper, where it is mixed and dosed by the dosing screws' rotary motion. The material is also sheared between the screws and the barrel wall as it moves through the system. Key parameters like screw speed, feed rate, and temperature in different system zones can be precisely controlled, making continuous slurry production via TSE highly promising.^[3,9–11] The resulting slurry's rheological properties,^[12] e.g., dynamic viscosity, are influenced by the screw configuration. Further important process parameters are screw speed, throughput, volume flow, filling degree, and residence time distribution (RTD).^[2] In particular, the knowledge of the RTD is important to efficiently reject scrap, which is 5% and more of the total material used,^[13,14] while maximizing resource utilization and ensuring traceability.^[1]

However, the continuous mixing process makes it difficult to define product batches. Because there are no longer natural

S. Otte, J. Maelger, S. Schabel, J. Fleischer
wbk Institute of Production Science
Karlsruhe Institute of Technology
76131 Karlsruhe, Germany
E-mail: simon.otte@kit.edu

H. Nirschl
Institute of Mechanical Process Engineering and Mechanics
Karlsruhe Institute of Technology
76131 Karlsruhe, Germany

 The ORCID identification number(s) for the author(s) of this article can be found under <https://doi.org/10.1002/ente.202402196>.

© 2025 The Author(s). Energy Technology published by Wiley-VCH GmbH. This is an open access article under the terms of the Creative Commons Attribution License, which permits use, distribution and reproduction in any medium, provided the original work is properly cited.

DOI: 10.1002/ente.202402196

batches, it is more difficult to associate process data with the product, and complex material and batch mixtures are created.^[15,16] This is relevant for two important scenarios: material often can still be used for a certain period of time after an unforeseen fluctuation in the dosing system since the consequences of the dosing fluctuation do not reach the extruder outlet only after a certain dead time in the production. Without knowledge of the residence time in the process, it is not possible to eject nonconforming material precisely and at the same time in a resource-efficient manner. However, the slurry traceability during mixing is not yet possible, as the battery cell or its components' traceability is only possible from the coating process onward. In Addition, knowing how long the material remains in the mixing process is also important for optimization and automation.

Dankwerts' method describes material behavior in a process, including residence time and distribution for continuous processes.^[17] The residence time is defined as the time t that an element spends in a system and provides a way to quantitatively describe flows through system components.^[18] Since the residence time of individual elements varies, the RTD function $E(t)$ is introduced. This normalized distribution function describes the temporal distribution of material elements in the system and provides a probability distribution of residence times.^[19] By integrating function $E(t)$, the amount of material that has left at time t is obtained.^[20,21] The cumulative distribution curve $F(t)$ indicates the probability that the residence time of an element is at most t , or the fraction of elements that have left the system by time t . It follows that $F(0) = 0$ and $F(\infty) = 1$.^[22] The distribution function $E(t)$ is characterized by the mean residence time t_m . Since the RTD is a statistical probability distribution, t_m can be calculated using the first-order statistical moment.^[23]

The RTD can be determined experimentally or by simulation. Experimental determination of the RTD is done by adding a tracer. The tracer is added to the system in a defined amount and for a defined time t_T , hereafter the input concentration $C_{in}(t)$ is measured. Afterward, the concentration of the tracer at the outlet of the system, hereafter referred to as the outlet concentration $C_{out}(t)$, is measured over time t . If the input concentration $C_{in}(t)$ is not ideal, $E(t)$ can be calculated by separate measurement of $C_{in}(t)$ and subsequent mathematical deconvolution.^[24]

According to ref. [25], the following conditions must be met to analyze a system with the RTD: 1) The process is continuous with constant mass flow at the system boundaries. 2) The mass flows

at the input and output of the system are in a constant or periodic state. 3) The mass flows at the input and output are unidirectional, so there is only one exit from the system after the material and tracer enter. 4) The addition of tracer materials does not affect the overall flow of the system.

These considerations apply to both liquid and powder-based systems.

There are various techniques for tracer addition, including pulse, step, periodic, and stochastic addition. The progressions of $C_{in}(t)$ and $C_{out}(t)$ for pulse and step addition are shown in Figure 1.

Pulse injection has a linear increase in $C_{in}(t)$, which is similar to a Dirac pulse. Ideally, the tracer is added at the rate of the fluid flow so that the fluid flow is not affected and the tracer addition time must be negligibly small.^[26] In the case of an idealized pulse addition of the tracer, the duration is zero and the amount of tracer is infinite. Normalizing $C_{out}(t)$ results in $E(t)$.^[27]

For a step addition, $C_{in}(t)$ increases abruptly at t_0 . Unlike the pulse addition, $C_{in}(t)$ remains at the new value. $C_{out}(t)$ also increases with a delay. $C_{out}(t)$ rises with a delay and follows a normalized Fermi curve $F(t)$, representing a cumulative distribution function.

Pulsed tracer addition offers several advantages in experiments, like reducing the time required and required tracer quantity while minimizing effects on the flow properties of the system. Second, analysis of the shape of the $C_{out}(t)$ curve provides a direct indication of the mixing behavior of the system. However, determining the appropriate amount of tracer and adding it in a pulsed manner is challenging at high backmixing. For steady-state tracer addition, access to the open system must be ensured to allow accurate and reproducible addition. The tracer amount can be introduced into the system in advance. This simplifies the process. However, the larger tracer quantities have a bigger influence on the flow behavior and can distort it.^[28] Therefore, careful selection of the tracer is required when adding it in steps. A detailed comparison of pulsed and step addition is available in ref. [28].

For the continuous mixing process in battery cell production, Haarmann et al. carried out some experiments with different amounts of tracer.^[10] However, a systematic investigation of the RTD based on a statistical design of experiments has not yet been undertaken. Furthermore, the effect of screw speed, mass flow, and solid content on the mean residence time t_m and the RTD has not been studied.

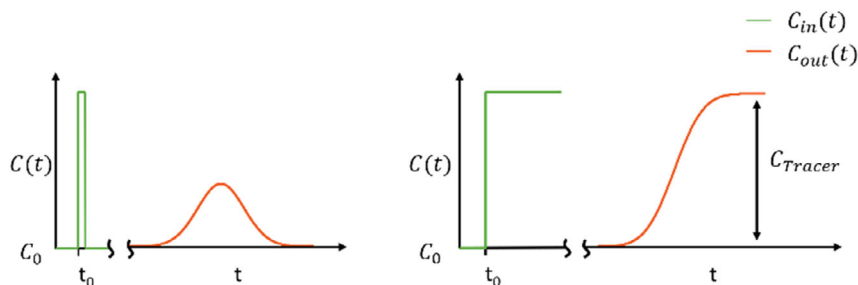


Figure 1. Visualization of the pulse (left) and step (right) response of a tracer and the system response.

2. State of the Art

A systematic literature review was done across several industries (e.g., food, pharmaceuticals, plastics). Selected studies were classified by industry, materials, plant components, tracer addition methods, and measurement techniques such as conductivity, NIR spectroscopy, and colorimetry. The most relevant references are discussed below.

Nassauer examines the NaCl concentration–conductivity relationship in RTD, showing that NaCl solutions up to 0.8% are suitable tracers due to their linear conductivity response.^[29]

English and Muzzio analyze a system with a feeder, continuous mixer, and tablet press. They measure each component's RTD and use convolution to calculate the overall RTD. The feeder has a narrow RTD, while the mixer has strong backmixing and a wide RTD, resulting in an overall RTD that is wider than any individual component.^[27] Leeb et al. investigated the RTD of corn semolina in a TSE. Both colored particles and NaCl are used as tracers and compared. A higher sensitivity was obtained with colored particles. The study found that solid content affects RTD width, while rotational speed affects mean residence time.^[30] Zhang et al. investigated the effects of different screws in the TSE with different speeds and mass flows. The RTDs of each screw element were then determined by mathematical deconvolution. Mass flow was found to have a greater influence on the RTD curve than screw speed.^[31] In their work, Escotet-Espinoza et al. demonstrated differences in the RTD of powders with different physical properties under identical process conditions. The system includes a feeder, mixer, and NIR camera for tracer measurement. For RTD experiments, tracer mass should stay below 5% of the steady-state mixer mass. In addition, optical control of the tracer addition is recommended to ensure immediate and complete introduction of the tracer. An inline method is recommended for real-time tracer detection, preventing overlap between successive additions.^[25,28] Kartunnen et al. and Escotet-Espinoza et al. recommend at least three tracer experiments to reduce variability. Understanding noise, measurement bias, and mass flow fluctuations is essential to minimize errors.^[21,28] Kartunnen et al. examined RTD measurement methods in three pharmaceutical tableting plants, comparing NIR and colorimetry for continuous mixing. Both are reliable, but pulsed tracer addition presents challenges. NIR requires costly and time-consuming calibration, while colorimetry is faster but sensitive to low concentrations. RTDs of individual components were measured and combined, assuming plug flow in the feeder and neglecting silo backmixing. Process parameters were held constant.^[21] Razavi et al. analyzed the influence of different tracer materials in the powder on the RTD curves. For this purpose, the flow properties of different tracer materials are systematically compared and the tracers are added to three different powders in two different mixers by pulse addition.^[32] Van Snick et al. investigated which powder properties affect RTD. Two layers are introduced above the feeder, one with a tracer. The maximum residence time is when the bottom layer exits, measured by NIR. The results show that the feeder type has a significant effect on the RTD, which requires experimental determination for each feeder.^[33,34]

Haarmann et al. investigated the RTD of the solvent in the continuous production of an anode slurry in a TSE. The system

for the continuous production of a battery slurry consists of a dosing unit that feeds the premixed powder, a positive displacement pump, which doses the liquid solvent, and the TSE. The RTD is measured by the pulse addition of a NaCl solution into the liquid dosing unit with an inline measurement of the conductivity at the outlet of the extruder. The tracer addition technique and the exact dosing point remain unclear. A linear relationship between an NaCl concentration of 30% in deionized water and conductivity is assumed but not validated. The amount of tracer increases with the volume flow (2 mL at 3 L h^{−1} and 3 mL at 4.5 L h^{−1}) in order to keep the level of the measurement signal constant. The process parameters selected as factors are the mass flow, the speed, and the screw configuration with a constant solid content of 48%. The factors are not varied according to a static experimental design and therefore no statistically valid statements can be made about the RTD behavior as a function of the factors. The RTD of the powder dosing unit and the liquid dosing unit in the mixing process is not determined.^[10]

The systematic literature search shows that no systematic investigation of RTD in the continuous mixing process of the electrode slurry has been carried out. The experimental determination of RTD is also insufficiently investigated compared to the pharmaceutical and food industries. Furthermore, it has not yet been possible to conclusively determine how big the influence of mass flow, solid content, and screw speed on the RTD is. Thus, an experimental RTD determination in the TSE plant with a systematic variation of the process parameters is essential in order to determine the effects of the parameter quantifiably.

3. Experimental Section

3.1. Materials

This study focuses on the processing of water-based anode slurries. As the active material graphite Mechano-Cap1P1 (HC Carbon GmbH, Germany) is used. The conductive additive is Super C65 conductive CB (Nanografi Nano Technology, Turkey), while the binders were carboxymethylcellulose (CMC) (Carl Roth, Germany) with a degree of substitution of 0.85 and styrene-butadiene rubber (SBR, Nanografi Nano Technology, Turkey). The dry components were homogenized using a drum hoop mixer (Type MINI-II, J. Engelsmann AG, Germany). To minimize variations in feed homogeneity, all experiments were conducted using the same batch of dry components.

3.2. Experimental Setup

The plant for continuous mixing consists of the TSE ZSK 18 MEGAlab (ZSK 18 mL) (Coperion GmbH, Germany) and can be divided into several subsystems (**Figure 2**). The two liquid dosing systems (blue and green) for the solvent water and a mixture of solvent and SBR are identical in design and consist of a tank with a type NM005BY extruder screw pump of the company Netzsch (Germany) connected to it and a hose connection to the process section. The powder is dosed in the powder dosing unit (yellow). This consists of a tank with an agitator for

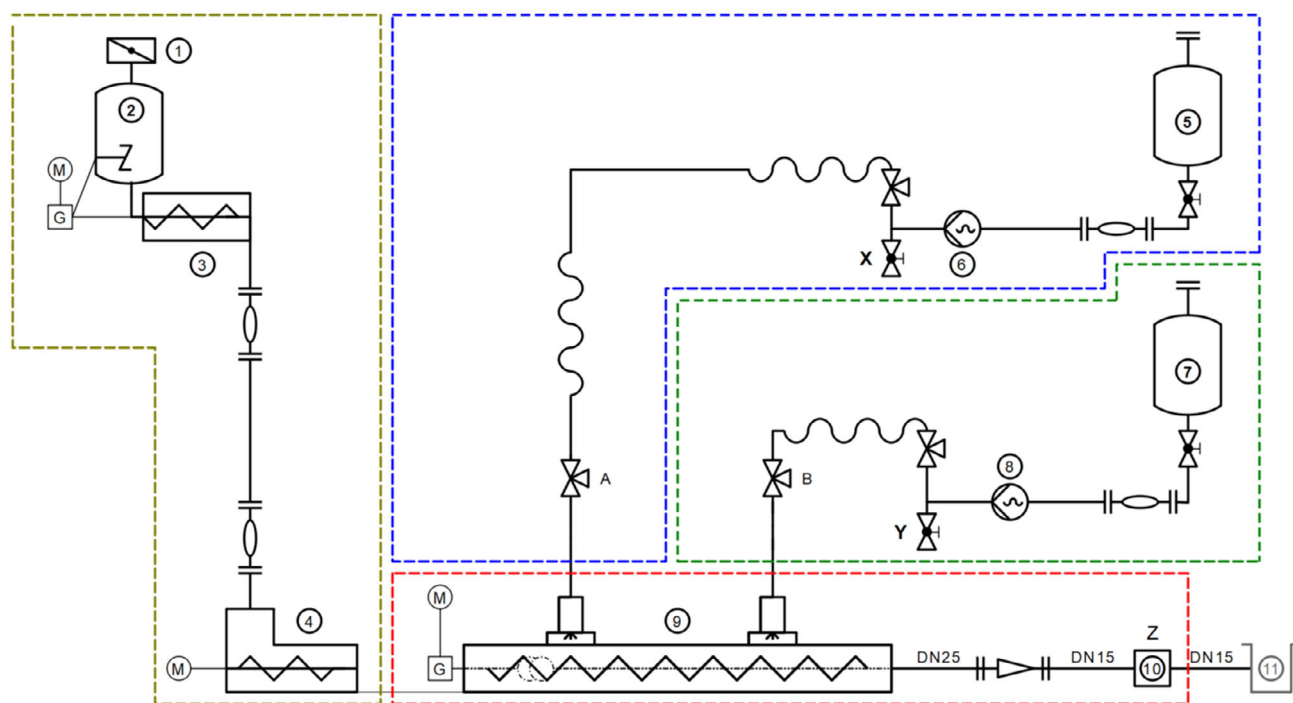


Figure 2. P&I diagram of the TSE of the type ZSK 18 mL. Powder dosing unit (yellow), solvent dosing unit (blue), binder dosing unit (green), and TSE (red). The tracer addition positions are marked A–E. The position of the conductivity sensor is labeled with X, Y, Z.

homogenization and a gravimetric powder dosing unit with twin screws in the Pharma QT20 version from Coperion GmbH (Germany).

The core of the system is the ZSK 18 mL TSE. The two screws rotate in the same direction and are made up of kneading, shearing, backmixing (blue), and conveying (green and orange) elements with different pitches (**Figure 3**).

The conductivity is measured inline using a conductivity sensor type 8221 from Christian Bürkert GmbH & Co. KG (Germany) with a measuring range from 0.1 to $500.000 \mu\text{S cm}^{-1}$. The conductivity sensor consists of two current electrodes and two voltage electrodes. The electrodes are aligned in the direction of flow. The sensor has a cell constant of 0.153733 cm^{-1} and a resolution of $18 \mu\text{S cm}^{-1}$ at a measuring frequency of 10 Hz.

To minimize air-induced measurement errors, the 3D printed polylactide measurement tube was developed. The lowest deviation occurred with an S-fitting with an inner diameter of 24 mm, which reduces air entrapment in the ascending slurry flow and minimizes pipe interference with conductivity measurements.

The final setup of the measuring section is shown in **Figure 4**. After the slurry leaves the process section (1) in a DN25 pipe, the diameter is reduced to the pipe diameter DN15 (2) required for

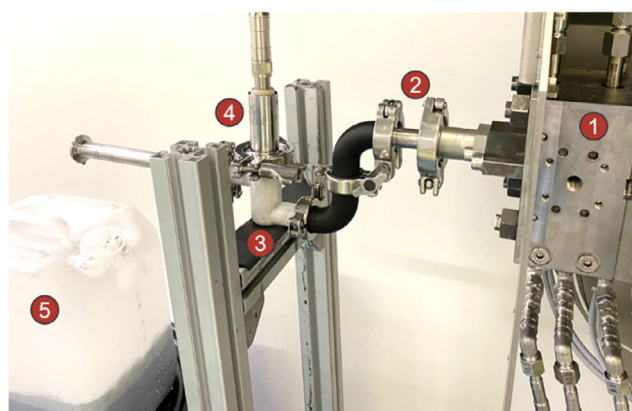


Figure 4. Setup of the measuring section with conductivity sensor.

the measuring equipment. This is followed by a step downward to prevent backflow into the TSE. The conductivity sensor is connected via the S-fitting (3). The slurry is discharged into a collecting tank (5) through a DN15 pipe.

Before the experiments, the feeder hoppers were fully loaded to ensure uninterrupted operation. RTD tests were conducted

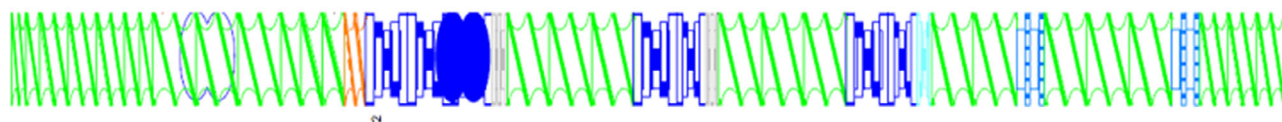


Figure 3. Screw configuration of ZSK 18MI.

under controlled conditions to minimize any impact from external disturbances, maintaining a process temperature of 22.5 °C. In every experiment, the TSE line handled untraced powders for at least two mean residence time to ensure a stable operating state was reached. Data from the TSE and conductivity sensor were recorded at 10 Hz using a Siemens PLC (Simatic S7-1500, 6ES7517-3AP00-0AB0) from Siemens AG (Germany) and MATLAB R2021a from The MathWorks Inc. (USA) via an OPC UA interface.

3.3. Design of Experiment

For the design of experiment (DoE), the number of trials was reduced to a minimum using a standardized experimental design in order to reduce the necessary amount of resources to a minimum. Partial factorial experimental designs were used because they require as few trials as possible with minimal loss of information. For this purpose, only a subset of the possible combinations of factors and levels is examined. A quadratic regression model was used in which the quadratic terms of the main effects are supplemented.^[35] It is calculated using the following Equation (1) with the coefficients β and the factors x_{1i} and x_{2i} :

$$y_i = \beta_0 + \beta_1 x_{1i} + \beta_2 x_{2i} + \beta_{11} x_{1i}^2 + \beta_{12} x_{1i} x_{2i} + \beta_{22} x_{2i}^2 + \varepsilon_i \quad (1)$$

Two experimental designs were developed, one based on the central composite design (CCD) and one based on the Box–Behnken design (BBD). The reason for this decision is that the authors could not determine in advance with certainty

whether an extension factor $\alpha > 1$ would lead to problems in carrying out the experimental design since the factor space is restricted by real process limits. CCD offers the advantage of a constant prediction variance since the design can be rotated while maintaining a given extension factor α . The testing effort, and therefore the time and resources required, increases. The BBD requires a lower number of runs, which increases efficiency. It is also more robust to measurement errors than the CCD. However, orthogonality and rotatability are not guaranteed.

The three factors (mass flow, screw speed, and solid content of the slurry) are investigated. A mass flow of 2–20 kg h^{−1} and a screw speed of 300–1200 rpm are defined by the plant limits. The technical process limits allow a solid content of 10–60%. As shown in **Figure 5**, the cube of the BBD is identical to the cube of the CCD, which also covers the extremes in the corners and star points. The validation of the feasibility of the experiment points with the process simulation from ref. [9] shows that there are no process-critical points in the CCD. The experiment points for BBD and CCD are listed in Table A1 and A2, Appendix.

To determine the RTD, the conductivity was manipulated using a tracer. For the solvent and the binder dosing unit, 5 mL of a 1 mol L^{−1} NaCl solution as tracer was injected as a pulse at the bottom of tank 5 or 7 using a syringe and the change in conductivity at position X or Y was measured (Figure 2). In the TSE, 2 mL of a 1 mol L^{−1} NaCl solution was used as the tracer, which was added as a pulse at position A and position B using a syringe. The addition of the tracer to determine the RTD of the binder solution (position B) takes place at a later time than the addition of the tracer to determine the RTD of the process part

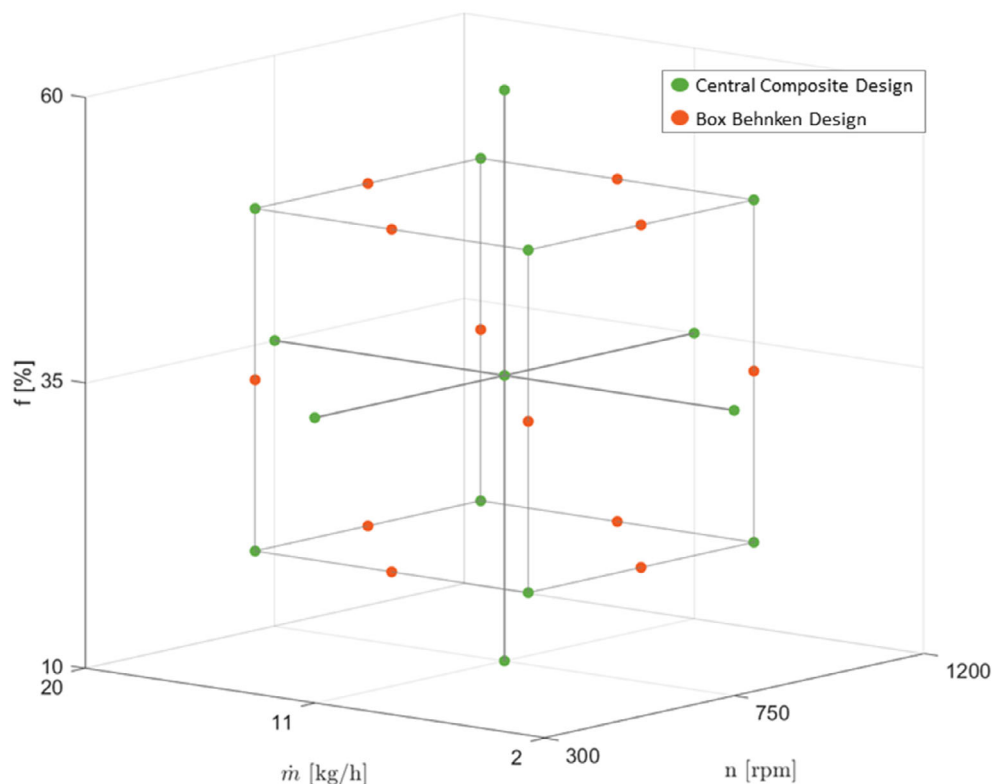


Figure 5. Statistical experiment plans CCD (green) and BBD (orange) of the experimental determination of the RTD in the TSE.

(position A), so that the conductivity curves do not influence each other. The change in conductivity was measured at position Z (Figure 2). Tracer injections and measurements were carried out 3 times for each point of the CCD and BBD. The new tracer was only injected once the conductivity had returned to its original starting level, thus ensuring that no more tracer was present in the process.

For the RTD of the powder dosing unit, a pulse (25 g) of sodium hydrogen carbonate was placed in tank 2 at the top of the agitator at a filling level of 2.5 kg. Subsequently, 5.0 kg of the premix was added. The conductivity was measured at position Z.

4. Results

In the first step, the material's characterization will be described. This is necessary to select a suitable tracer for determining the RTD and is shown in the second subsection. The experiment results are presented in the third subsection. Finally, the reproducibility of the experiments and the validity of the findings obtained are considered.

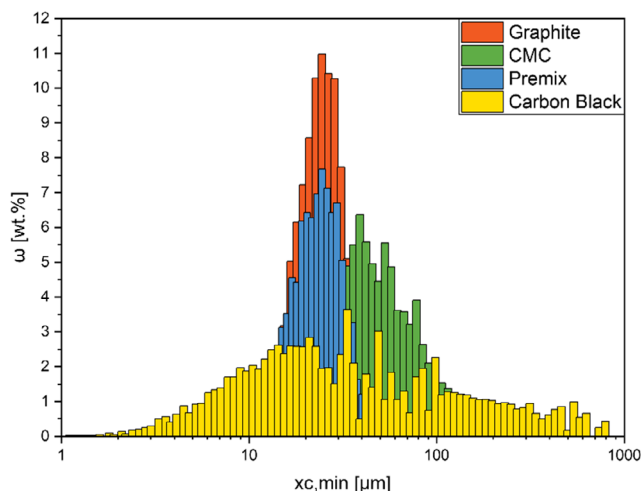


Figure 6. PSD of graphite, CMC, CB, and premix.

4.1. Material Characterization

The particle size distribution (PSD) of the powders was characterized with a Camsizer X2 (Microtrac Retsch GmbH, Germany). Using dry dispersion measurements, the PSD can be determined in the range of 1 μm to 8 mm. The size definition $x_{c,min}$ is selected. $x_{c,min}$ is the particle width determined from the narrowest of all measured chords x_c . Graphite (orange) makes up the majority of the premix (blue); therefore, the PSD of graphite and premix is almost identical with a median D50 of 22.74 μm for premix and 23.15 μm for graphite (Figure 6). The PSD of the CMC (green) is wider compared to the PSD of the premix, with a rightward shift of the median D50 to 40.42 μm . The CB (yellow) has a similar median to the premix at 26.16 μm , but a broader distribution.

For further characterization, scanning electron microscopy (SEM) images are taken with a JSM 6010Plus/LW scanning electron microscope (JEOL, Germany) with a secondary electron detector. Figure 7 (left) shows an SEM image of graphite at 400x magnification. The particle size on the SEM images corresponds to the PSD in the figure. The graphite particles are platelet-shaped with a flaky structure. The SEM image in Figure 7 (right) shows that CMC has a porous structure with voids and a rough surface texture. Both individual elongated particles and agglomerates can be seen.

A measurement of the viscosity of the binder mixture and the slurry is relevant to the selection of the tracer. The viscosity of the binder mixture and the anode slurry is determined using a HAAKE MARS rheometer from Thermo Scientific (Germany). A sample is applied to a glass plate, and the shear rate $\dot{\gamma}$ is gradually increased to 1200 s^{-1} at constant intervals. The temperature was kept constant at 20 $^{\circ}\text{C}$ during the measurements. The measurement result of the binder mixture shows a linear curve of shear stress τ with a mean dynamic viscosity η of 2.7945 mPas (Figure 8). It has a low viscosity and has the properties of a Newtonian fluid.

To determine the viscosity of the anode slurry (DoE point BBD10), the shear rate $\dot{\gamma}$ was increased from 0.25 to 1200 s^{-1} at constant intervals. Figure 9 shows the curve of the shear stress τ calculated from the torque. As the shear rate $\dot{\gamma}$ increases, the dynamic viscosity η decreases. The curve is not linear, so the fluid is non-Newtonian and shear thinning.

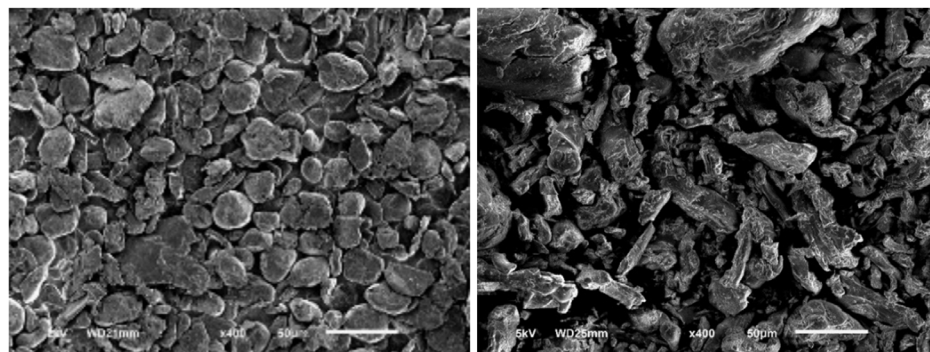


Figure 7. SEM image of MechanoCap 1P1 (left) and CMC (right).

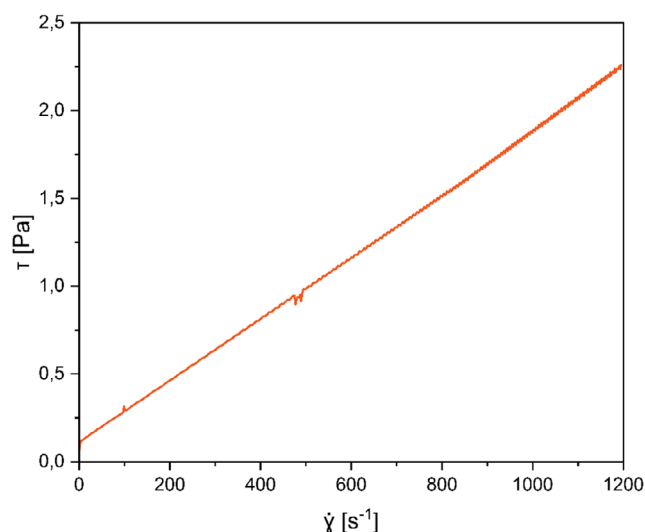


Figure 8. Shear rate as a function of the shear stress of the SBR binder mixture with 15 wt% SBR.

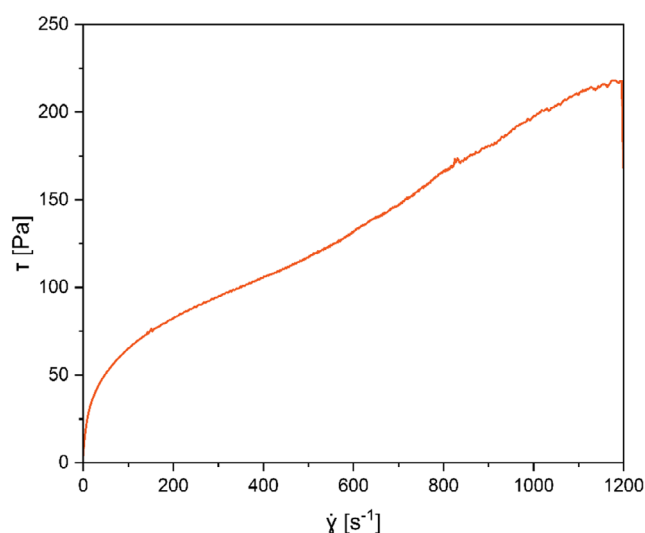


Figure 9. Shear rate as a function of the shear stress of the anode slurry with solid content of 35%.

4.2. Tracer Selection

The selected tracer should fulfil several issues such as a tracer should not be reactive and should not be absorbed in the system. In addition, the tracer should dissolve completely in the medium so that it follows the same trajectory through the system as the other materials. Furthermore, there should be a linear relationship with the tracer concentration and it should be detectable at low concentrations. Once added, the tracer should ideally be homogeneously distributed throughout the entire cross section. In order for the tracer to be reliably detected, it must differ from the other materials or the base substance in at least one physical property. However, the behavior of the tracer should deviate as little as possible from the other material properties, e.g., the PSD

should be comparable.^[18] In the case of fluids, similar density and viscosity should also be ensured.^[21] If these criteria are met, the flow behavior of the tracer will be comparable to the flow behavior of the fluid or powder under investigation.

The reference medium determines the choice of tracer. A liquid tracer is suitable for characterizing the solvent dosing unit, binder dosing unit, and TSE, as these are liquid systems. In contrast, a powder tracer is needed to characterize the powder flow behavior and the RTD of the powder feeder system.

The binder solvent and slurry are turbid liquids. Therefore, a fluorescence-based tracer is unsuitable because the required accuracy cannot be achieved.^[29] The use of a radioactive tracer requires considerable metrological effort. Colorimetric methods are unsuitable because the black anode slurry only shows a measurable color difference at very high tracer concentrations, which would strongly influence the flow properties. Therefore, conductivity measurement is chosen as the measurement method. Possible tracers are aqueous solutions and acids with high conductivity, an HCl or NaCl solution. A solution of 1 mol L⁻¹ NaCl concentration has a conductivity of 81.420 S cm⁻¹ and can be measured at low concentrations in slurry. It is nonreactive and will not be adsorbed in the process. Unlike HCl, it does not attack the plant components, such as the twin screws. The NaCl solution also meets the requirement for complete solubility in the materials of the anode slurry. According to ref. [36], an approximate linear relationship between conductivity and concentration can be assumed for a NaCl concentration of 1 mol L⁻¹. To determine the required amount of tracer, the measured conductivity values for the 1/2/5/10 mL tracer volumes were compared in an iterative process. The results confirmed the linear relationship observed by ref. [36]. It was also shown that even 2 mL reliably causes a sufficiently large change in conductivity at both minimum and maximum mass flow in the TSE. For the dosing systems, 5 mL was selected because the residence times are longer and therefore the mixing behavior is greater, requiring a higher concentration of tracer. To further validate the tracer quantity, its influence on the rheological properties of the slurry was tested. Samples of the slurry with and without the tracer (1 mol L⁻¹ NaCl solution) were taken at the outlet of the TSE and rheologically analyzed using the HAAKE MARS rheometer.

The viscosity measurements of anode slurry at 35% solid content without (orange curve) and with 2 mL of the 1 mol L⁻¹ NaCl solution as tracer (blue curve) illustrate the viscosity after adding, while maintaining a constant solid content shows a decrease in viscosity with increasing shear rates (Figure 10). Therefore, the slurry with tracer and the anode slurry without tracer are a shear-thinning fluid. The curve of anode slurry with tracer is slightly lower due to the low viscosity of the NaCl solution. This corresponds to an absolute deviation of 0.06082 Pa s at a shear rate $\dot{\gamma}$ of 1000 s⁻¹. Therefore, it can be assumed that the flow properties of the slurry with and without NaCl solution are approximately identical. The tracer method is thus valid for determining the RTD in the TSE.

The literature suggests that pulsed tracer addition is suitable for measuring RTD in fluids. Pulse addition offers simple, high-resolution data acquisition because backmixing is less than with step addition. Pulse addition minimizes the effect of the tracer on the slurry properties due to the lower amount used, while step

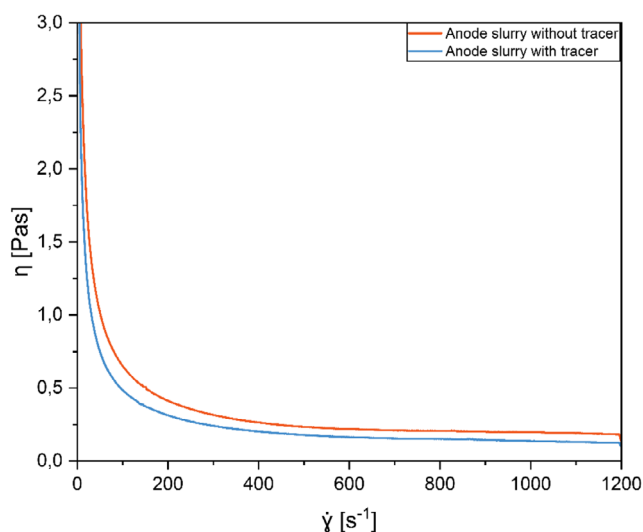


Figure 10. Comparison of the viscosity of an anode slurry with a solid content of 35% without and with tracer (1 mol L⁻¹ NaCl solution).

addition is more difficult to implement operationally. The pulse addition method was chosen to determine the RTD of the fluids in the TSE system.

For the powder dosing system, finely sieved NaCl powder, powdered sugar, and sodium bicarbonate powder were compared as potential tracer materials. Powdered sugar and NaCl are nonreactive and have a high solubility in water. The PSD of the powders was compared to the premix to determine their flow behavior, as shown in **Figure 11**. The median is 57.58 μm for powdered sugar, 165.36 μm for extra-fine NaCl, and 95.11 μm for sodium bicarbonate. All medians are different from the median of the premix. The PSD of the premix overlaps with that of powdered sugar, while there is minimal overlap between the PSD of the premix and NaCl. Sieving with a 25 μm mesh sieve tower using ultrasonic excitation was unsuccessful because the

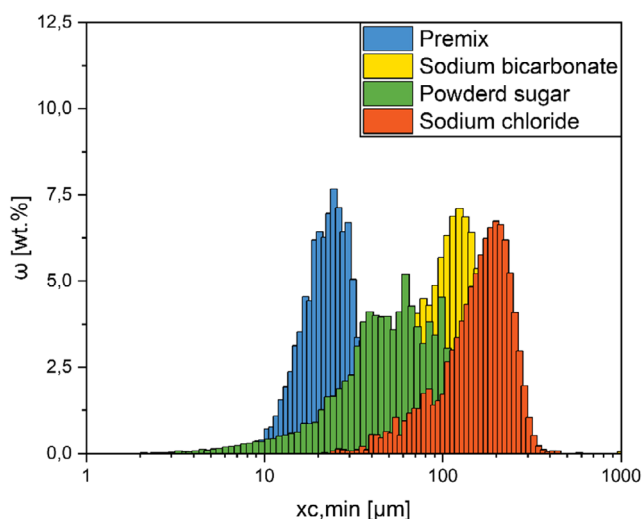


Figure 11. Comparison of the PSD of premix (blue), powdered sugar (green), finely sieved NaCl (orange), and sodium bicarbonate (yellow).

proportion of NaCl particles smaller than 50 μm was only 4.2%. Furthermore, it was not possible to measure reliable conductivity changes during the experiments due to strong backmixing effects in the extruder. Therefore, NaCl was not considered further.

Next, the particle shape of powdered sugar and sodium bicarbonate was examined. As shown in the SEM images (**Figure 12**), both materials have a similar particle structure.

Powdered sugar particles have an irregular, angular shape. Many of the particles are flat and plate-like with sharp edges. This structure is typical of powdered sugar produced by mechanical grinding of sugar crystals. The surface of the particles is smooth and partially covered by smaller aggregates, which may indicate surface impurities. The particle size is up to 20 μm, which is similar to the particle size of the premix.

Sodium bicarbonate particles also have an angular and irregular shape. The surface of the particles is sometimes smooth and sometimes highly textured with rod-like structures (**Figure 13**). The edges of the particles vary from round to sharp-edged. In addition to the medium and large particles, there are also significantly smaller particles. Closer inspection gave the impression that these were fragments of larger particles because they often have a smooth rather than a rod-shaped structure on the surface. The average particle size is 95.11 μm; the amount of particles smaller than 50 μm was only 19.07%.

Based on the results obtained so far, the change in conductivity at a defined concentration of the materials sodium bicarbonate and powdered sugar and the influence on the viscosity of the slurry were investigated. In order to determine the powdered sugar content in the premix at which a significant change in the initial concentration $C_{out}(t)$ can be measured, the dependence of the conductivity of the slurry on the powdered sugar content and the sodium bicarbonate content in the premix is studied. The linearity of tracer concentration and conductivity is also investigated. For this purpose, five samples were mixed with 100 g of slurry with a defined gravimetric tracer content of 1/2.5/5/10/20% in the premix. The results of the off-line conductivity measurement are shown in **Table 1**. The addition of 10% powdered sugar causes a drop-in conductivity of 578 μS cm⁻¹. Considering the minimum resolution of the conductivity sensor of 18.08 μS cm⁻¹, a powdered sugar content of 20% in the premix is considered reasonable for the modified recipe. The conductivity difference of the slurry in the offline measurement is 828 μS cm⁻¹. However, the sodium bicarbonate shows a much larger change in conductivity at a much lower tracer concentration. Even 1% tracer leads to a 2.5-fold increase in conductivity, at 2.5% it is almost 4.5-fold. This shows that even the smallest amounts are sufficient to change the target value sufficiently.

The PSD of the individual tracers differs from the distribution of the premix. Therefore, premixes with the corresponding tracer proportions were prepared and compared in terms of their PSD. As shown in **Figure 14**, the PSD is within distribution windows of similar size. However, the 20% powdered sugar premix has a slightly wider PSD than the standard premix. A premix with 1% sodium bicarbonate has an almost identical PSD. This is due to the very low tracer content, which causes little change in the PSD. Sodium bicarbonate is therefore preferred to powdered sugar as a tracer. This decision considers that an increased amount of

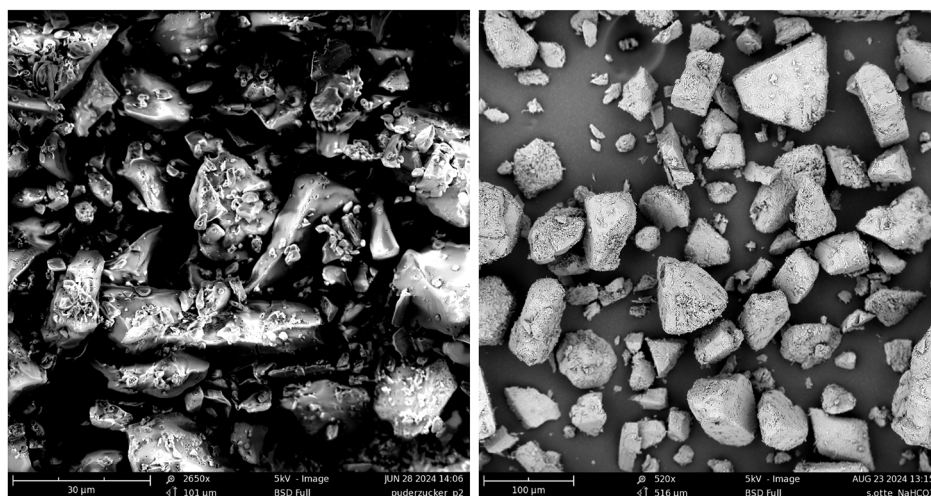


Figure 12. SEM image of powdered sugar (left) and sodium bicarbonate (right).



Figure 13. SEM image with 2650x magnification of sodium bicarbonate. The surface is unstructured and rough with individual rod-like structures.

tracer could have a greater influence on the flow properties of the mixture.

Finally, the influence of powdered sugar and sodium bicarbonate on the viscosity was investigated. The solid content of the slurry with and without tracer is 35% to ensure comparability.

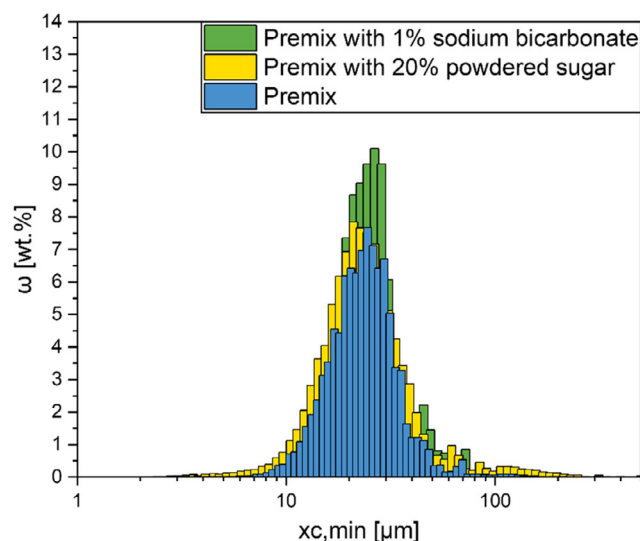


Figure 14. Comparison of the PSD of premix with and without tracers.

All curves show a decrease in viscosity η for increasing shear rates $\dot{\gamma}$, but the flow behavior of the anode slurry with and without tracer is not identical (**Figure 15**). The blue and green curves are slightly shifted downward. For powdered sugar (blue), an absolute deviation of 0.06319 Pas for a shear rate $\dot{\gamma}$ of 1000 s^{-1} is measurable. It can be concluded from this that the flow properties of the slurry with and without powdered sugar are almost similar.

Table 1. Comparison of the conductivity of slurry at different concentrations of the tracers powdered sugar and sodium bicarbonate.

Tracer	Conductivity [$\mu\text{S cm}^{-1}$] with specified gravimetric component; basic conductivity $1848 \mu\text{S cm}^{-1}$				
	1%	2.5%	5%	10%	20%
Powdered sugar	1626	1556	1468	1270	1020
Sodium bicarbonate	4650	8223	12 190	20 370	35 280

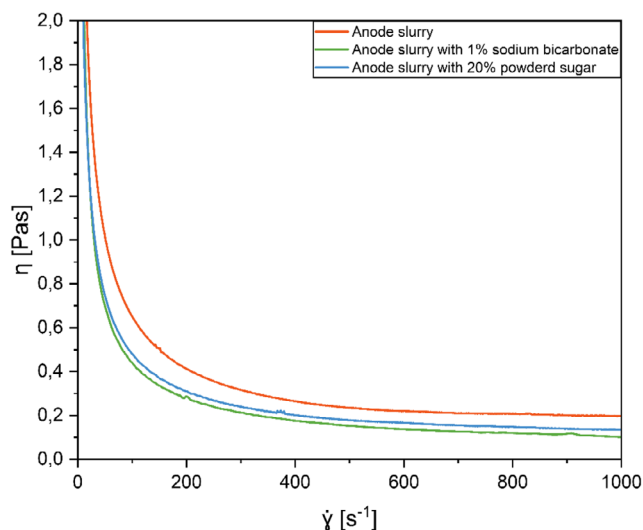


Figure 15. Comparison of the viscosity of anode slurry with a solid content of 35% with and without tracer.

Even with slurry with 1% baking soda, a deviation can be detected that even exceeds the deviation of slurry with powdered sugar. Thus, when using sodium bicarbonate, the absolute deviation is 0.09606 Pa s at a shear rate $\dot{\gamma}$ of 1000 s⁻¹. Nevertheless, the assumption that the flow behavior of the premix and sodium bicarbonate is similar can still be made. Thus, sodium bicarbonate appears to be a suitable tracer for the premix in the dosing unit.

4.3. RTD in Process Section

The conductivity curves are recorded for all experimental points according to the DoE. The process parameters screw speed, mass flow, and solid content are varied and the tracer is added after the process has reached a steady state. All of the recorded curves were found to be similar in principle, showing a beta distribution. The typical RTD characteristic of the slurry in the TSE with process parameters from the center of the factor space (CCD10, screw speed 750 rpm, mass flow 11 kg h⁻¹, solid content 35%) as a response of pulsed addition of 2 mL tracer (1 mol L⁻¹ NaCl solution) at time $t = 0$ s at position A (Figure 2) is shown in Figure 16.

The curve has a very steep, almost vertical rise up to the maximum conductivity. After that, the curve drops exponentially and the conductivity approaches the base conductivity again. The curve can be characterized by the 4 times t_{\min} , t_{peak} , t_m , and t_{\max} . The time t_{\min} is the minimum residence time, sometimes referred to in the literature as the delay time and indicates the time until the conductivity increases sharply. The minimum residence time is determined by a gradient. The required threshold was set to 3. When the gradient of the RTD curve exceeds this value, t_{\min} is reached. The delay time t_{\min} of the RTD curve shown is 30.9 s. The minimum residence time describes the time that elapses until the first fluid element from the dosing in the TSE reaches the outlet. The peak residence time indicates the

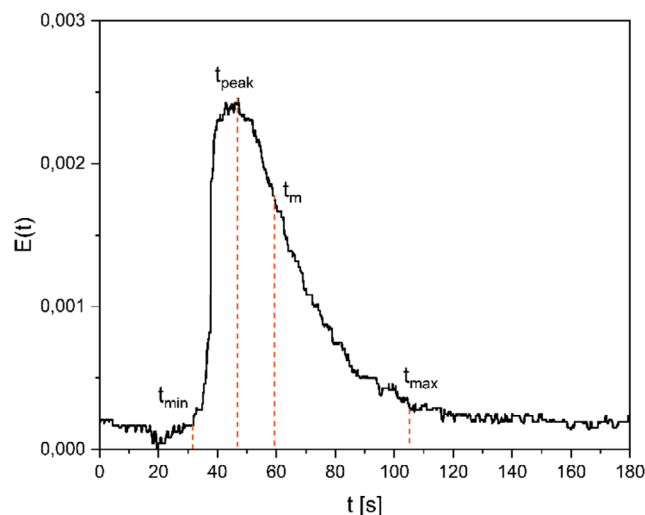


Figure 16. Response of the conductivity for one experiment point with a screw speed of 750 rpm, mass flow of 11 kg h⁻¹, and a solid content of 35% (CCD10) after tracer addition (2 mL of 1 mol L⁻¹ NaCl solution) as a pulse at $t = 0$ s.

most likely residence time t of a fluid element. In the RTD curve shown, t_{peak} is 45.59 s. The mean residence time t_m of this RTD is 59.26 s. At this time, exactly half of the fluid elements—in this case, of the tracer—have left the TSE. Another characteristic is the maximum residence time t_{\max} . It is defined as the time t at which the slope of the RTD curve after t_{peak} becomes greater than a defined negative threshold. The threshold for the maximum residence time t_{\max} was set to -0.1 . The maximum residence time of this RTD curve is 102.62 s. The probability of a fluid element remaining in the TSE longer than t_{\max} is negligible.

In order to analyze the influence of each of the parameters on the RTD, one of the parameters was varied while the other two parameters were kept constant. Figure 17 shows how the RTD changes as the screw speed is varied with a constant mass flow of 11 kg h⁻¹ and a solid content of 35%. The yellow curve shows the RTD slurry in the TSE at a screw speed of 300 rpm. Compared to the reference curve, the center of the factor space (blue), the yellow curve is shifted to the right and has a wider spread. This indicates a higher residence time with higher backmixing at lower screw speeds. The mean residence time t_m of the yellow curve is 79.46 s. The green curve shows the RTD of an experiment point at a maximum screw speed of 1200 rpm. Compared to the blue curve, the green curve has a narrower distribution with a shift to the left. The mean residence time t_m of the green curve is 52.46 s. The shift of the green curve is smaller than the shift of the yellow curve, despite an identical difference in screw speed. This indicates a nonlinear relationship between changes in velocity and the resulting changes in residence time. As screw speed decreases, RTD spread and backmixing increase.

The RTD curves of the slurry in the TSE for the three different solid content 10% (CCD6, yellow), 35% (CCD10, blue), and 60% (CCD7, green) are shown in Figure 18. The screw speed for all three points is 750 rpm and the mass flow is 11 kg h⁻¹. The RTD curve of 10% solid content is located to the left of the RTD of the reference curve, CCD10. The mean residence time t_m of the

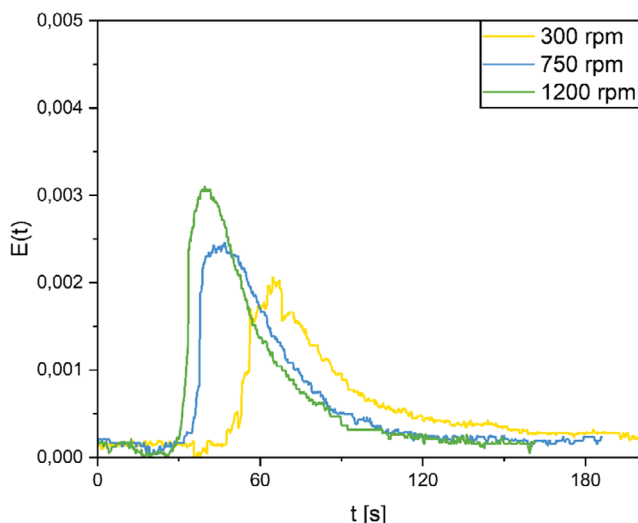


Figure 17. RTD curves of the slurry in the TSE with 35% solid content and mass flow of 11 kg h^{-1} for screw speed with 300 rpm (yellow curve), 750 rpm (blue curve), and 1200 rpm (green curve).

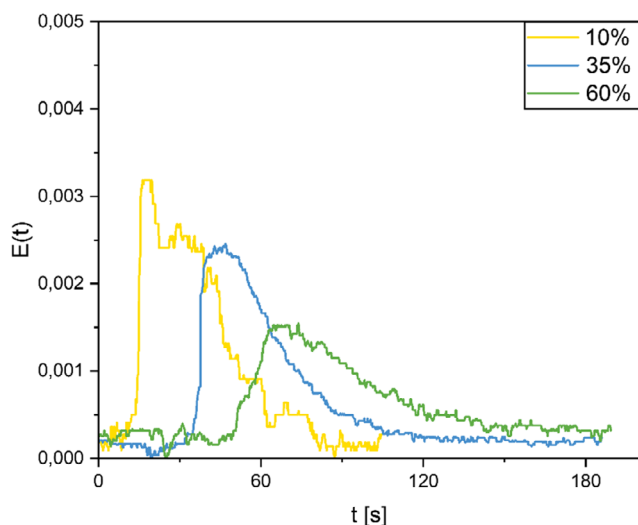


Figure 18. RTD curves of the slurry in the TSE with screw speed of 750 rpm and mass flow of 11 kg h^{-1} for solid content of 10% (yellow curve), 35% (blue curve), and 60% (green curve).

yellow curve is 32.83 s, which is the shortest residence time of all experiment points. The maximum is at $t_{\text{peak}} = 17.2 \text{ s}$. The green curve represents the RTD for 60% solid content with a maximum at $t_{\text{peak}} = 66 \text{ s}$. The green curve shows a significantly larger scatter and a longer dwell time than the RTD of the center point. From this comparison, it can be concluded that the residence time of the slurry in the TSE decreases as the solid content decreases. The higher the solid content of the slurry, the longer the slurry remains in the TSE.

The graph in **Figure 19** shows the RTD for three different mass flows: 2 kg h^{-1} (CCD8, yellow), 11 kg h^{-1} (CCD10, blue), and 20 kg h^{-1} (CCD9, green). The screw speed for all points

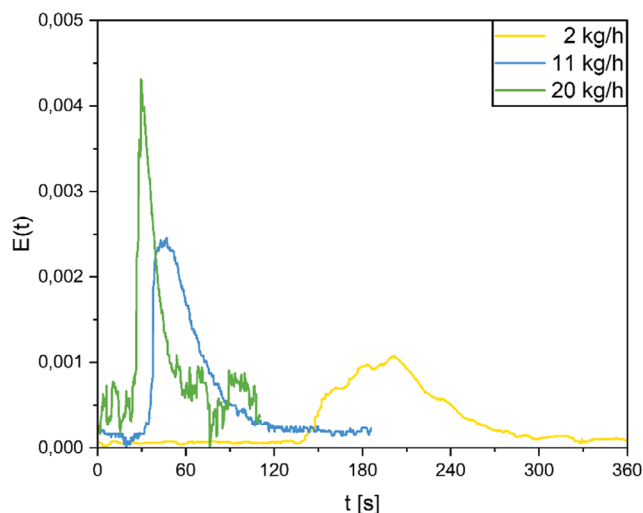


Figure 19. RTD curves of the slurry in the TSE with screw speed of 750 rpm and solid content of 35% for mass flow of 2 kg h^{-1} (yellow curve), 11 kg h^{-1} (blue curve), and 20 kg h^{-1} (green curve).

shown is 750 rpm and the solid content is 35%. For the mass flow of 2 kg h^{-1} , the yellow RTD curve shows a flatter distribution with a late maximum at 201 s. This distribution indicates a longer residence time of the particles in the system. The mean residence time $t_m = 203.12 \text{ s}$ is 3.4 times higher than the mean residence time t_m of the center of the factor space (blue). The yellow RTD curve has the highest mean residence time t_m of all experiment points. In contrast, the green RTD curve ($\dot{m} = 20 \text{ kg h}^{-1}$) shows an early and narrow maximum at 29.77 s. This indicates that the particles pass through the system much faster. The mean residence time of 39.27 s is 33% shorter than that of the center point CCD10. The green curve shows oscillations at the end, which can be explained by the sampling rate and the measurement frequency. It can be deduced that the residence time decreases with increasing mass flow. The higher the mass flow, the shorter the residence time of the slurry in the TSE, but the relationship between mass flow and average residence time is nonlinear. Lower mass flows seem to have a greater influence on the RTD than higher mass flows.

4.4. RTD in Liquid Systems

Changing the screw speed in the process section has no effect on the liquid dosing systems. The mass flow of the liquid dosing unit is only defined by the mass flow in the TSE and the solid content of the slurry. This results in the following minimum (min), mean (m), and maximum (max) mass flow rates for solvent ($\dot{m}_{\text{H}_2\text{O}}$) and binder solution (\dot{m}_{SBR}) (**Table 2**).

Figure 20 shows the raw data of the conductivity measurements of the solvent dosing unit at minimum $\dot{m}_{\text{H}_2\text{O,min}}$, mean $\dot{m}_{\text{H}_2\text{O,m}}$, and maximum water mass flow $\dot{m}_{\text{H}_2\text{O,max}}$. The tracer addition of 2 mL NaCl solution is done for all curves at $t = 0 \text{ s}$. The green curve shows the conductivity for the minimum deionized water mass flow $\dot{m}_{\text{H}_2\text{O,min}}$. The conductivity does not change for a time $t_{\text{min,min}} = 509 \text{ s}$ and is approximately zero.

Table 2. Mass flow rates for the liquid dosing system of the solvent water ($\dot{m}_{\text{H}_2\text{O}}$) and binder solution (\dot{m}_{SBR}).

	$\dot{m}_{\text{H}_2\text{O}}$ [kg h ⁻¹]	\dot{m}_{SBR} [kg h ⁻¹]
Min	1.15	0.17
Mean	5.41	1.10
Max	9.67	2.03

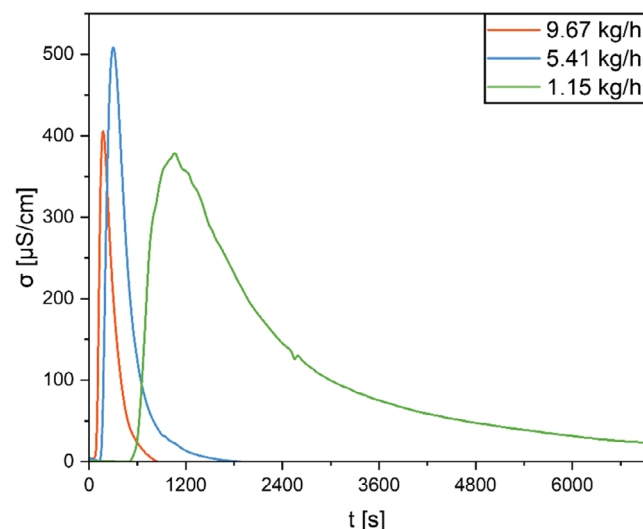


Figure 20. Conductivity measurement during tracer addition in the liquid dosing unit with deionized water with varying mass flow.

After $t_{\text{min,min}}$, the curve increases rapidly, the conductivity peak of $380.16 \mu\text{S cm}^{-1}$ is at $t_{\text{peak,min}} = 1064 \text{ s}$, and then decreases slowly. The curve runs over a longer period of time with a continuous decrease in conductivity. The mean residence time is $t_{\text{m,min}} = 1806 \text{ s}$. The blue curve represents the course of the

conductivity after the addition of the tracer for the average deionized water mass flow $\dot{m}_{\text{H}_2\text{O,m}}$. This curve reaches a maximum conductivity of $513.09 \mu\text{S cm}^{-1}$ at $t_{\text{peak,m}} = 295 \text{ s}$ and then decreases faster than the green curve. This indicates a higher mass flow with less backmixing. The curve returns to the base conductivity at $t_{\text{max,m}} = 1741 \text{ s}$. The orange curve shows the conductivity for the maximum mass flow $\dot{m}_{\text{H}_2\text{O,max}}$ with $t_{\text{min,max}} = 97 \text{ s}$. After $t_{\text{peak,max}} = 171 \text{ s}$, the orange curve reaches the maximum conductivity value of $416.11 \mu\text{S cm}^{-1}$. The orange curve stays at this high level for a shorter time and falls more quickly than the blue curve. The different courses of the curves illustrate the influence of mass flow on the residence time of the tracer in the liquid dispenser. Higher mass flows result in a shorter residence time and a faster drop in conductivity, indicating less backmixing.

4.5. RTD in Powder Dosing System

Changing the speed of the twin screws does not affect the feed rate of the powder dosing unit, which is only determined by the solid content and the mass flow of the entire system. Therefore, the mass flows are $\dot{m}_{\text{powder,min}} = 1.09 \text{ kg h}^{-1}$, $\dot{m}_{\text{powder,m}} = 4.47 \text{ kg h}^{-1}$, and $\dot{m}_{\text{powder,max}} = 7.85 \text{ kg h}^{-1}$.

After the addition of the tracer, a response curve is obtained that is significantly different from the response curves of the other subsystems (Figure 21, left). After a short time, a steep increase in the curve occurs for all curves. This is followed by the global maximum of the curve and a steep decrease near the base conductivity. It should be noted that the first peak in the curve shows a low level of variation. After the first peak, the curves show individual small peaks and the average conductivity is significantly above the base conductivity. The number and height of the peaks show no pattern, nor does the time between peaks. On closer inspection, however, a curvature can be seen that is overlaid by several peaks. This is the second characteristic feature of the RTD curve and becomes particularly apparent when the curves are smoothed (Figure 21, right).

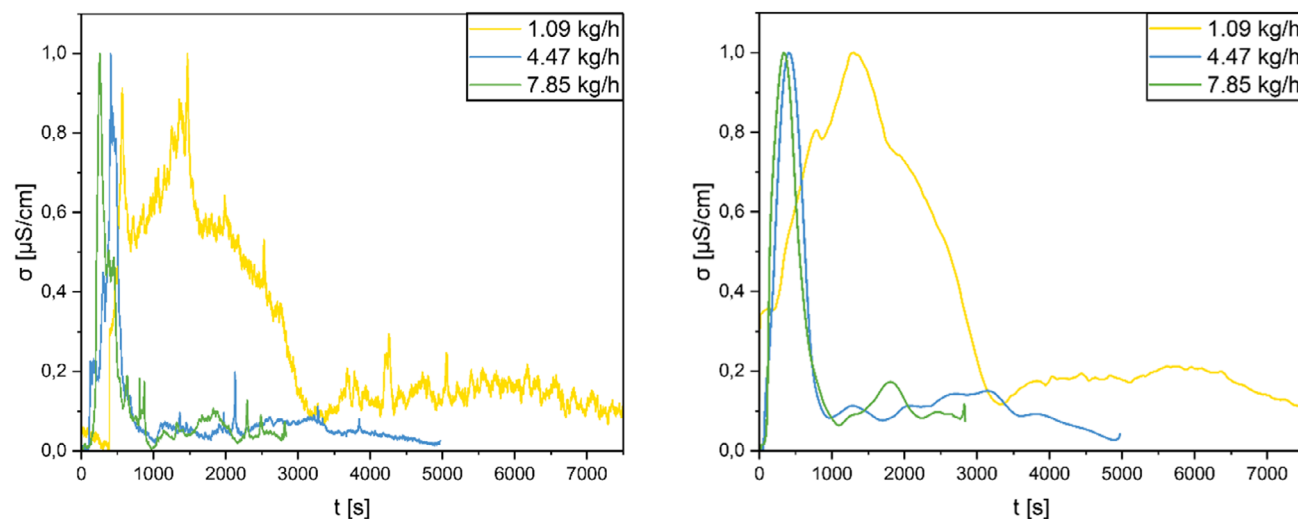


Figure 21. Raw RTD curves (left) and smoothed RTD curves (right) of the powder dosing system in combination with the TSE for minimum (yellow curve), maximum (green curve), and mean mass flow (blue curve).

Table 3. Characteristic RTD times of the powder dosing system.

	t_{\min} [s]	t_{peak} [s]	t_m [s]	t_{cur} [s]	t_{\max} [s]
Min	279	1469	6336	5050	8691
Mean	103	345	481	1219	2820
Max	129	253	454	1825	2774

The base conductivity is reached only after the curvature. In most cases, a final peak can be seen in the last section, where the conductivity deviation from the base is small.

The influence of the mass flow on the RTD of the power mixing system can be clearly seen. As the mass flow increases, the characteristic times decrease. The following characteristic times are obtained for the minimum (min), mean (m), and maximum (max) mass flow (Table 3).

5. Discussion

The relevance and validity of the obtained results are discussed below, starting with the confirmation that the tracer addition occurred in a pulse-like manner. According to ref. [23], the pulse-like addition time of the tracer should be at most 1% of t_m to be considered an ideal pulse. The recorded tracer addition durations were recorded and checked for this (Figure 22). The analysis shows that the average tracer addition time is 0.65 s. With an average residence time of the fluids in the mixing process of 59.26 s at test point CCD10, this results in an average valid addition time of 0.59 s. The actual average addition time of 0.06 s is slightly above the recommended addition time, which may be due to manual tracer addition and manual signal acquisition of the start and end time of tracer addition. However, this slight deviation allows the addition to be considered an ideal pulse.

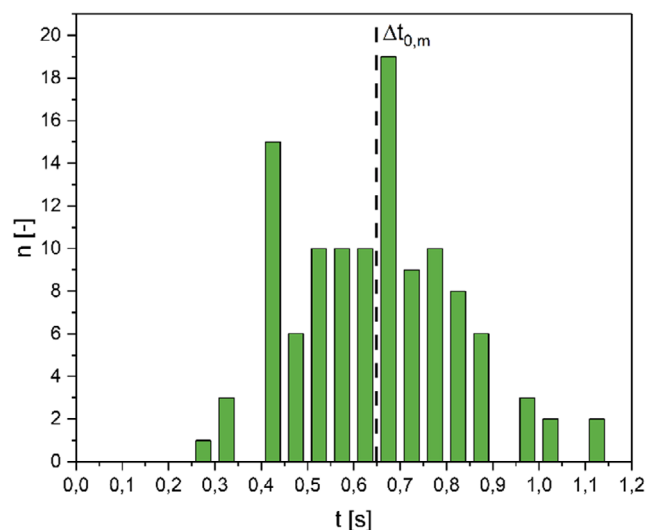


Figure 22. Duration of tracer addition for all points (BBD and CCD) to experimentally determine the RTD of the slurry in the extruder. The average addition time is 0.65 s.

The next step is to evaluate the reproducibility of the RTD and measurements (Figure 23). Each curve represents the response of the liquid dosing unit to a pulsed tracer addition of 5 mL of NaCl solution. The results show a high degree of agreement in the times t_{\min} and rise curves, with a slight variation in the maximum conductivity values at t_{peak} . However, this variation does not significantly affect the RTD, as the relative values are important.

The reproducibility of the measurement results was also verified for the TSE by comparing the averaged conductivity curves for the center points of the factor space (Figure 24). The center of the factor space is at a screw speed of 750 rpm, a mass flow of 11 kg h⁻¹, and a solid content of 35%. The average residence time is 53.49 s with a standard deviation of 4.47 s. Again, there

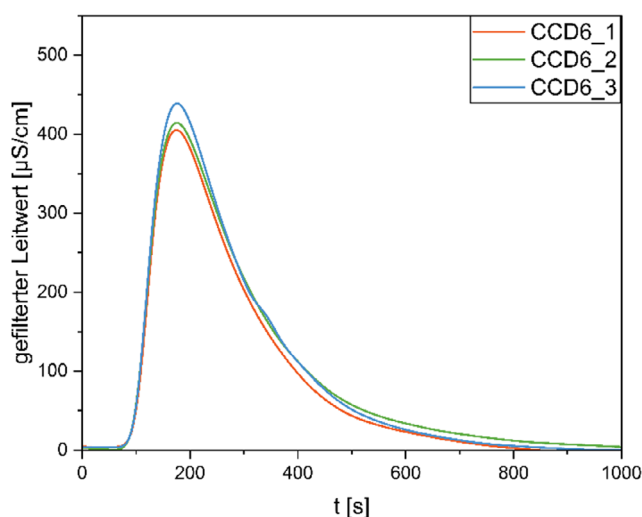


Figure 23. Comparison of the conductivity curves of the solvent water in the liquid dosing unit at a maximum water mass flow rate.

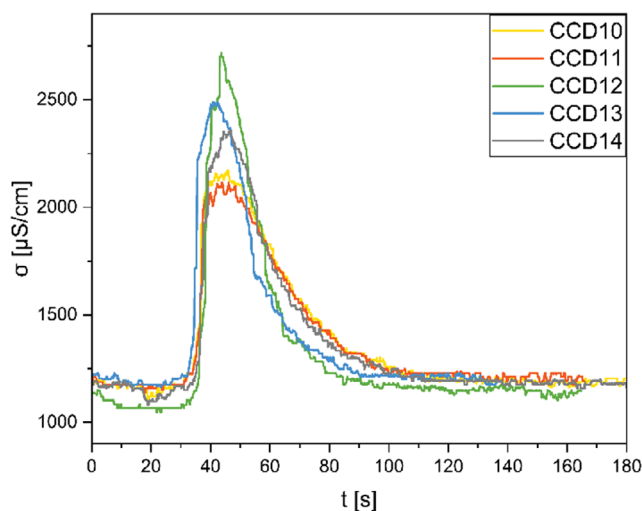


Figure 24. Comparison of the averaged RTD curves for the center point of the factor space for the process section of the extruder.

is a high repeatability between the individual measurements, confirming the reproducibility.

After confirming the pulsed tracer addition and the reproducibility of the RTD curves, the influence of screw speed, mass flow, and solid content is analyzed. Contour plots are used to further determine the interactions of screw speed, mass flow, and solid content on the mean residence time t_m of the slurry in the TSE. These plots provide a clear way to illustrate the dependencies and influences of the parameters. The mean residence time t_m is selected as the most characteristic parameter of the RTD for analysis. The first contour diagram (Figure 25) shows the relationship between screw speed and mass flow. It can be seen that low screw speed and low mass flow lead to higher mean residence time t_m . These areas are shown in green. With increasing screw speed and mass flow, the mean residence time decreases, as shown by the transition from green to blue. The progression of the color changes indicates that both parameters have a significant influence on the residence time. In particular, it can be seen that an increase in screw speed at constant mass flow leads to a decrease in the mean residence time. Similarly, an increase in mass flow at constant screw speed results in a decrease in residence time.

The second contour diagram (Figure 26) shows the interaction between screw speed and solid content. Low screw speed and a low solid content result in shorter residence time, which is

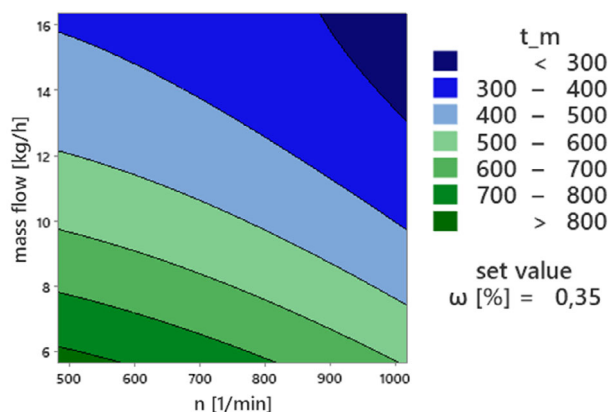


Figure 25. Contour plot for the interaction of mass flow and screw speed with t_m for the BBD model.

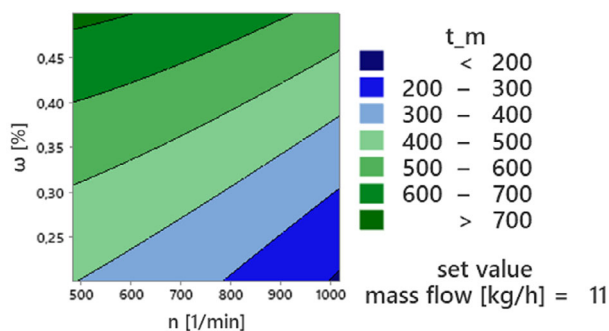


Figure 26. Contour plot for the interaction of solid content and screw speed with t_m for the BBD model.

represented by blue areas. With increasing screw speed and increasing solid content, t_m increases. The influence of the solid content on the residence time is more significant than the influence of the screw speed, as can be seen from the steeper color gradients. This indicates that a higher solid content at constant screw speed results in a significant increase in mean residence time.

The third contour plot (Figure 27) illustrates the relationship between mass flow and solid content. Low values of both parameters result in shorter residence times, represented by the blue areas. With increasing mass flow and solid content, the residence time t_m increases. Both process parameters show a strong and nearly linear interaction on the residence time. Increasing the solid content at constant mass flow significantly increases the mean residence time. A higher mass flow rate combined with a higher solid content causes a further increase in residence time.

This shows that all three parameters have significant and sometimes complex effects on the residence time. While increasing screw speed or mass flow will decrease residence time, increasing solid content will increase residence time. Screw speed had less influence than the other two parameters. However, it is important to note that the effect of screw speed on the RTD can vary depending on the screw configuration. For example, a different screw configuration with the same speed and otherwise the same parameters may result in a shortening or lengthening of the t_m and thus a change in the RTD.

The RTD curves of the powder dosing system are not as sharp as the RTD curves of the TSE or the liquid dosing system. The individual peaks are caused by a partially increased concentration of the tracer. On the one hand, this could be related to agglomerates, which the authors consider rather unlikely. On the other hand, it could be related to the flow behavior of the powder in the storage container. It is very likely that there is a core flow in the powder dosing unit. If it is a mass flow, the first peak would be larger and the bulge smaller. Similarly, if it is mass flow, the curve would be similar to the curves of the liquid dosing systems. Core flow causes peaks to occur again and again after the first peak: The material at the edge slides down like an avalanche, causing uneven dripping. The resulting higher concentration of tracer mixes with other material in the TSE to form a peak.

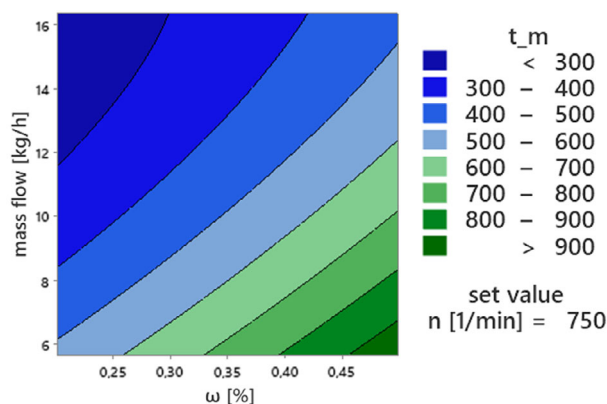


Figure 27. Contour plot for the interaction of mass flow and solid content with t_m for the BBD model.

Since the material sliding down is random, this also explains why the smaller peaks occur at irregular intervals. The curvature indicates that the tracer is well mixed in the storage vessel. A vertical agitator is installed in the hopper to prevent material bridges at an early stage. However, the geometry of the agitator also mixes the powder in the hopper, resulting in a mostly homogeneous powder mixture. Only after some time, i.e., when a lot of powder has been dosed, does the concentration of the tracer in the premix decrease because a low concentration is continuously “diluted” with new powder.

Another point to consider is the effect of air in the system, particularly on the conductivity measurement. Air bubbles cause a short decrease in conductivity even though the slurry remains unchanged (Figure 28). This creates measurement noise that negatively affects the accuracy of the measurements. The foaming behavior of the binder solution has a worsening effect here. This was considered when defining the measurement section. Several options were considered and the one with the lowest noise was chosen. Nevertheless, a variation up to $160 \mu\text{S cm}^{-1}$ can be observed. These variations are much smaller than the expression of a peak. Therefore, the validity of the results presented here can still be assumed. However, to obtain even more accurate results, it is recommended to take further measures to reduce air bubbles.

When the RTD curves were investigated, there was a significant difference in the quality of the curves. In particular, the results at the extremes and at the process limits showed fluctuations. It was found that the star points for the CCD had to be repeated several times because the process was being operated at or beyond the process limits. While the repeated tracer experiments showed strong fluctuations, the results at the corner points and edge centers were very well reproducible. This confirms that the process was in a stable state at these points. Therefore, the authors recommend a DoE according to the BBD for a detailed investigation of the residence time behavior.

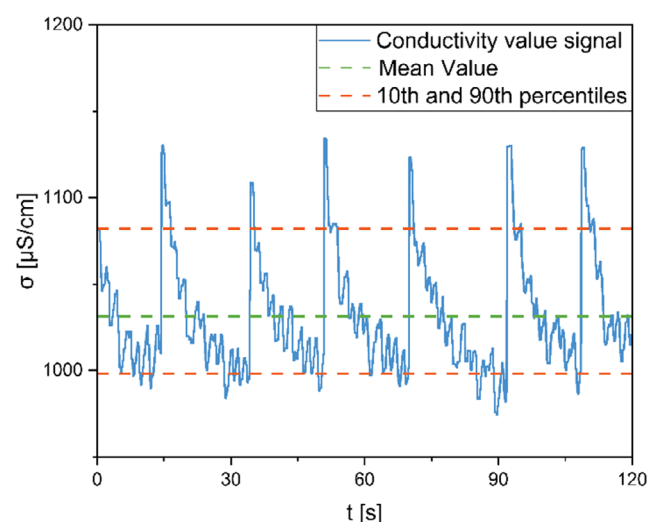


Figure 28. Variation of the conductivity due to air bubbles in the slurry. The mean value (green dashed line) is $1031.42 \mu\text{S cm}^{-1}$, the 10th percentile (lower orange dashed line) is $998.05 \mu\text{S cm}^{-1}$, and the 90th percentile (upper orange dashed line) is $1082.10 \mu\text{S cm}^{-1}$.

If the cube size is chosen correctly, the space of common parameter pairings is also covered. Prior to the study, care was taken to ensure that all common mass flows and solid contents were included in the DoE cube.

6. Conclusion

The RTD in the continuous mixing process for the production of a homogeneous battery AM is investigated for the first time in a systematic way. For this purpose, the materials are characterized and suitable tracers are selected. It is shown that 2 mL of a 1 mol L^{-1} NaCl solution is a suitable tracer for the TSE and that there is no significant impairment of the process. Sodium bicarbonate is selected as the tracer for the powder dosing system because it behaves most similar to the powder. For the first time, a systematic variation of the parameters screw speed, mass flow, and solid content is carried out and the effect on the residence time is determined. Mass flow has the greatest effect, followed by the solid content, while screw speed has a smaller effect. Based on the results presented, it is now possible to make an initial estimation of the expected minimum and maximum residence time. This makes it possible to eject defective material in a more resource-efficient manner. Furthermore, the control systems for the continuous mixing process can react adaptively to the residence time and reduce unnecessary control activities, leading to a more stable process control.

The RTD could be further investigated by varying other parameters such as screw configuration or formulation of the slurry. Similarly, it should be considered how to model the residence time distribution. In this case, it is important to investigate the accuracy of the prediction.

Appendix

Table A1. Experimental points of the BBD.

Point	n [rpm]	Mass flow [kg h^{-1}]	ω [%]
BBD1	482.43	11.00	20
BBD2	482.43	11.00	50
BBD3	482.43	5.65	35
BBD4	482.43	16.35	35
BBD5	750.00	5.65	20
BBD6	750.00	5.65	50
BBD7	750.00	16.35	20
BBD8	750.00	16.35	50
BBD9	750.00	11.00	35
BBD10	750.00	11.00	35
BBD11	750.00	11.00	35
BBD12	1017.57	11.00	20
BBD13	1017.57	11.00	50
BBD14	1017.57	5.65	35
BBD15	1017.57	16.35	35

Table A2. Experimental points of the CCD.

Received: November 19, 2024

Revised: January 31, 2025

Published online:

Point	n [rpm]	Mass flow [kg h^{-1}]	ω [%]
CCD1	300.00	11.00	35
CCD2	482.43	5.65	20
CCD3	482.43	5.65	50
CCD4	482.43	16.35	20
CCD5	482.43	16.35	50
CCD6	750.00	11.00	10
CCD7	750.00	11.00	60
CCD8	750.00	2.00	35
CCD9	750.00	20.00	35
CCD10	750.00	11.00	35
CCD11	750.00	11.00	35
CCD12	750.00	11.00	35
CCD13	750.00	11.00	35
CCD14	750.00	11.00	35
CCD15	750.00	11.00	35
CCD16	1017.57	5.65	20
CCD17	1017.57	5.65	50
CCD18	1017.57	16.35	20
CCD19	1017.57	16.35	50
CCD20	1200.00	11.00	35

Acknowledgements

The authors would like to express their appreciation to the German Federal Ministry of Education and Research (BMBF) for supporting the project “IntelliPast” (funding code: 03XP0343A) and the project “Agiobat2” (funding code: 03XP0369A). This work contributes to the research performed at KIT-BATEC (KIT Battery Technology Center) and at CELEST (Center for Electrochemical Energy Storage Ulm Karlsruhe).

Conflict of Interest

The authors declare no conflict of interest.

Author Contributions

Simon Otte: conceptualization; methodology; formal analysis; visualization; writing—original draft preparation. **Simon Otte** and **Julia Maelger:** investigation; validation. **Jürgen Fleischer** and **Hermann Nirschl:** resources. **Simon Otte**, **Sebastian Schabel**, **Hermann Nirschl**, and **Jürgen Fleischer:** writing—review and editing. **Jürgen Fleischer:** supervision and funding.

Data Availability Statement

The data that support the findings of this study are available from the corresponding author upon reasonable request.

Keywords

battery cell productions, continuous processes, design of experiments, mixing, residence time distributions, slurries, traceability

- [1] VDMA Batterieproduktion, *Roadmap Batterie-Produktionsmittel 2030: Update 2023*, **2023**.
- [2] H. Dreger, H. Bockholt, W. Haselrieder, A. Kwade, *J. Electron. Mater.* **2015**, *44*, 4434.
- [3] J. Li, J. Fleetwood, W. B. Hawley, W. Kays, *Chem. Rev.* **2022**, *122*, 903.
- [4] S. N. Bryntesen, A. Stromman, I. Tolstorebrov, P. Shearing, J. Lamb, O. S. Burheim, Opportunities for the state-of-the-art production of LIB electrodes—a review, **2021**, undefined.
- [5] M. M. Nasr, M. Krumme, Y. Matsuda, B. L. Trout, C. Badman, S. Mascia, C. L. Cooney, K. D. Jensen, A. Florence, C. Johnston, K. Konstantinov, S. L. Lee, *J. Pharm. Sci.* **2017**, *106*, 3199.
- [6] M. Haarmann, W. Haselrieder, A. Kwade, Extrusion-based processing of cathodes: influence of solid content on suspension and electrode properties, **2019**, undefined.
- [7] M. Keppeler, H.-Y. Tran, W. Braunwarth, *Energy Technol.* **2021**, *9*, 2100132.
- [8] J. F. Meza Gonzalez, H. Nirschl, F. Rhein, *Batteries* **2024**, *10*, 145.
- [9] M. Haarmann, D. Griebel, A. Kwade, Continuous processing of cathode slurry by extrusion for lithium-ion batteries, **2021**, undefined.
- [10] J. F. Meza Gonzalez, H. Nirschl, *Energy Technol.* **2023**, *11*, 1.
- [11] J.-H. Schünemann, H. Dreger, H. Bockholt, A. Kwade, *ECS Trans.* **2016**, *73*, 153.
- [12] S. Otte, N. N. A. M. Sufian, S. Schabel, J. Fleischer, *Energy Technol.* **2024**, *12*, 2400493.
- [13] P. Wunderlich, N. Ehteshami-Flammer, J. Krauß, A. Fitzner, L. Mohring, C. Dahmen, The Power of Digitalization in Battery Cell Manufacturing, **2024**.
- [14] M. Kehr, M. Locke, C. Offermanns, H. Heimes, A. Kampker, *Energy Technol.* **2021**, *9*, 2001113.
- [15] A. Buss, J. P. Doppler, I. Effenberger, D. Ensling, C. Haar, S. Hartleif, G. Riexinger, K. Schöbel, M. Trierweiler, T. Bauernhansl, in *Handbook on Smart Battery Cell Manufacturing: The Power of Digitalization* (Eds: P. Birke, M. Weeber, M. Oberle), World Scientific, New Jersey, London, Singapore, Beijing, Shanghai, Hong Kong, Taipei, Chennai, Tokyo **2022**, pp. 123–147.
- [16] G. Riexinger, J. P. Doppler, C. Haar, M. Trierweiler, A. Buss, K. Schöbel, D. Ensling, T. Bauernhansl, *Proc. CIRP* **2020**, *93*, 125.
- [17] P. V. Danckwerts, *Chem. Eng. Sci.* **1953**, *50*, 3857.
- [18] J. M. Winterbottom, M. B. King, in *Reactor Design for Chemical Engineers*, 1st ed., Thornes, Cheltenham **1999**.
- [19] J. Peng, H. E. Huff, F. Hsieh, *J. Food Process. Preserv.* **1994**, *18*, 263.
- [20] E. Salamí, *Dissertation*, Eidgenössische Technische Hochschule Zürich, Zürich **1968**.
- [21] A.-P. Karttunen, T. R. Hörmann, F. Leersnyder, J. de Ketolainen, T. Beer, W.-K. de Hsiao, O. Korhonen, *Int. J. Pharm.* **2019**, *563*, 184.
- [22] E. B. Nauman, *Chem. Eng. Commun.* **1981**, *8*, 53.
- [23] L. Fillaudeau, K. Le-Nguyen, C. André, *J. Food Eng.* **2009**, *95*, 489.
- [24] D.-I. J.-H. Ham, *Dissertation*, Technische Universität Chemnitz, Chemnitz **2003**.
- [25] M. S. Escotet-Espinoza, S. Moghtadernejad, S. Oka, Z. Wang, Y. Wang, A. Roman-Ospino, E. Schäfer, P. Cappuyns, I. van Assche, M. Futran, F. Muzzio, M. Ierapetritou, *Powder Technol.* **2019**, *344*, 525.

- [26] M. Baerns, A. Behr, A. Brehm, J. Grmehling, K.-O. Hinrichsen, H. Hofmann, R. Palkovits, U. Onken, A. Renken, Technische Chemie, Wiley-VCH, Weinheim **2013**.
- [27] W. Engisch, F. Muzzio, *J. Pharm. Innov.* **2016**, 11, 64.
- [28] M. S. Escotet-Espinoza, S. Moghtadernejad, S. Oka, Y. Wang, A. Roman-Ospino, E. Schäfer, P. Cappuyns, I. van Assche, M. Futran, M. Ierapetritou, F. Muzzio, *Powder Technol.* **2019**, 342, 744.
- [29] J. Nassauer, *Dissertation*, Technische Universität München, München **1978**.
- [30] C. V. Leeb, B. Maiser, H. P. Schuchmann, *Chemie Ingenieur Technik* **2008**, 80, 1175.
- [31] X.-M. Zhang, L.-F. Feng, S. Hoppe, G.-H. Hu, *Polym. Eng. Sci.* **2008**, 48, 19.
- [32] S. M. Razavi, A. D. Román-Ospino, P. Bhalode, J. Scicolone, G. Callegari, A. Dubey, A. Koolivand, S. Krull, G. Tian, X. Xu, T. O'Connor, M. Ierapetritou, F. Muzzio, *Powder Technol.* **2023**, 429, 118864.
- [33] B. van Snick, W. Grymonpré, J. Dhondt, K. Pandelaere, G. Di Pretoro, J. P. Remon, T. de Beer, C. Vervaet, V. Vanhoorne, *Int. J. Pharm.* **2018**, 549, 476.
- [34] B. van Snick, J. Dhondt, K. Pandelaere, J. Bertels, R. Mertens, D. Klingeleers, G. Di Pretoro, J. P. Remon, T. de Beer, C. Vervaet, V. Vanhoorne, *Int. J. Pharm.* **2018**, 549, 415.
- [35] K. Siebertz, D. van Bebbber, T. Hochkirchen, in *Statistische Versuchsplanung: Design of Experiments (DoE)*, 2nd ed., Springer Vieweg, Berlin, Heidelberg **2017**.
- [36] M. Wächter, in *Tabellenbuch der Chemie: Daten zur Analytik, Laborpraxis und Theorie ; [Viskosimetrie, Pyknometrie, Kryoskopie, Ebullioskopie, Spektroskopie]*, 1st ed., Wiley-VCH, Weinheim **2012**.